Remote terahertz spectroscopy from extended two-color plasma filaments: The ALTESSE 2 project

A. Talbi, B. Zhou, P. Jepsen, Stefan Skupin, A. Courjaud, L. Bergé

Remote terahertz spectroscopy from extended two-color plasma filaments: The ALTESSE 2 project

A. Talbi[1], B. Zhou[1], P.U. Jepsen[1], S. Skupin[2], A. Courjaud[3] and L. Bergé[4,5]

[1] *DTU Electro - Dept. Photonics Engineering, Technical University of Denmark, DK-2800 Kongens Lyngby, Denmark*
[2] *Institut Lumière Matière, UMR 5306 Université Lyon 1 - CNRS, Université de Lyon, 69622 Villeurbanne, France*
[3] *Amplitude, 11 Avenue de la Canteranne Cité de la Photonique, 33600 Pessac, France*
[4] *CEA, DAM, DIF - 91297 Arpajon - France*
[5] *Université Paris-Saclay, CEA, LMCE, 91680 Bruyères-le-Châtel, France*

PACS 42.65.Re – Ultrafast processes; optical pulse generation and pulse compression
PACS 32.80.Fb – Photoionization of atoms and ions
PACS 52.38.-r – Laser-plasma interactions

Abstract – Coherent time-domain spectroscopy (TDS) using terahertz radiation is valuable for fundamental science, security, and medical applications. This study investigates the performance of air-biased coherent detection terahertz spectroscopy (ABCD-THz) when an extended plasma filament is created in the air over long distances. We report on the latest results obtained within the follow-up of the ALTESSE project ["Air Laser-based TErahertz SpectroScopy of Explosives" - L. Bergé et al., EPL **126**, 24001 (2019)] whose objective is to measure a set of spectral signatures characterizing suspicious materials over meter-long distances. As one of the most critical steps towards routinely applying this technique, we verified the feasibility of a remote THz time-domain spectroscopy by loosely focusing two-color ultrashort laser pulses at more than 3 meters from the laser source. The absorption spectra of amino acids and explosives analyzed in such a filamentation geometry are compared with those obtained using a standard ABCD scheme where the plasma is generated at much shorter distances of ~ 30 cm.

Introduction. – Terahertz (THz) radiation located in-between microwave and infrared frequencies, belongs to the most exciting but less explored regions of the electromagnetic spectrum [1]. Non-metallic materials such as paper, plastics, clothes, wood, and ceramics are transparent to THz waves. On the other hand, THz radiation with meV photon energies is non-ionizing but strongly absorbed by water. Apart from the latter, many complex molecules have salient absorption features associated with vibrational and rotational transitions in this frequency range, providing unique fingerprints for spectral identification.

The remarkable potential for applications in this region of the electromagnetic spectrum has created a very active field of research since the 1990s, not only for spectroscopic purposes [2]. For instance, THz radiation makes it possible to envisage new non-invasive medical diagnostics [3], in particular for the detection of tumors [4, 5], and can even be used to trigger DNA demethylation in blood cancers [6]. THz waves also constitute suitable tools for the manipulation of material properties [7] by exploiting the dynamics of phonons and charge carriers in semiconductors, spin dynamics, superconductivity, THz-induced ferroelectricity, etc. Recent studies specifically require high THz fields to explore water dynamics emanating from the network of hydrogen bonds [8] or to perform pump-probe atom tomography of metal nanotips [9] with athermal evaporation. Broadband (≤ 20 THz) fields exceeding the GV.m^{-1} level moreover allow to catalyze chemical reactions on the surface of materials by triggering a collective response of atoms, as experienced at SLAC (Stanford Linear Accelerator Center) [10], where the THz fields were generated from coherent transition radiation through a solid target [11]. Controlling electric fields with amplitudes equal to or greater than 10 GV.m^{-1} is expected to act on chemical bonds selectively [12].

Among the most efficient emitters in the THz range, one can recall synchrotrons [13,14] and free electron lasers [15] where the curved trajectory of magnetically-deflected electrons generates synchrotron radiation in frequencies ranging from microwaves to X-rays. Besides, optically-driven

devices encompass photoconductive antennas [16, 17] and quantum cascade lasers [18,19], which can nowadays transmit frequencies around $1-5$ THz with powers up to one watt [20]. An efficient conversion mechanism is optical rectification [21] of a femtosecond laser pulse in an inorganic [22–24] or organic [25–28] electro-optical electro-optic crystal possessing a quadratic susceptibility $\chi^{(2)}$ [29]. By tilting the pump wavefront appropriately with respect to the laser propagation direction [30–32], such a mechanism can generate a planar THz wavefront with a conversion efficiency of up to 1%, energies close to one millijoule [33] and fields approaching the GV.m^{-1} level.

The previous techniques, however, supply THz spectra that are either narrowband or cover a limited spectral range below 5-6 THz. For optical rectification, for example, the spectral width is limited by phase-matching conditions and the fluence damage threshold of the crystal. Because the applications below require broad spectra, we focus on laser-induced filamentation in gases. Unlike nonlinear crystals and other solid materials, nonlinear interactions in gases have much fewer problems with damage thresholds as the gas either repairs or replenishes itself from a reservoir. As a result, gases can be driven at relatively high intensities and produce ultra-broadband THz spectra. In standard setups, a frequency-doubling crystal, such as barium borate (BBO), is used to generate a second harmonic (SH) beam from a fundamental beam (FH). Intense FH and SH pulses focused in the air to create a plasma are able to produce THz radiation from nonlinear processes dominantly driven by photocurrents [34,35]. This method supplies ultra-broadband spectra that span frequency ranges as wide as 0.1–200 THz [36]. Furthermore, for overall peak powers above the critical power for self-focusing $\sim 5-10$ GW [37], the regime of laser filamentation, reached through the interplay between Kerr self-focusing and plasma generation [37,38], makes it possible to generate THz pulses remotely in the atmosphere [39–41]. Extended THz-active channels of ionized air were demonstrated as 10-m long plasma regions at more than 50 meters from the laser exit by varying the focal distance of the pump pulse [41]. In general, plasma filaments can be triggered at longer distances exceeding several hundred meters [37], which offers a promising solution to generate THz radiation remotely, avoiding diffraction and absorption by water vapor. Last but not least, the energy contained in the THz pulse may be optimized by tuning the laser parameters, including the laser pump wavelength [42], pulse duration [43] and the number of harmonics in the pump pulse [44].

Characteristic frequencies of infrared-active molecular rotations and vibrations are detectable using the method known as THz time-domain spectroscopy (THz-TDS) [45, 46]. This technique, which aims to collect the absorption lines of a sample, is based on the interaction between a THz pulse and a probe laser pulse, whose delay is adjusted to measure point by point the temporal profile of the transmitted THz field. The THz electric field amplitude can then be measured using an electro-optical crystal (e.g., ZnTe crystal [47,48]) or by employing photoconductive antennas, which, however, rather suit relatively long THz pulses with limited bandwidths < 5 THz. To exploit broader THz spectra for spectroscopy measurements, detection by air nonlinearities may be preferable. When employing sources based on femtosecond laser pulses, particularly two-color femtosecond filaments, the THz beam is recombined with the optical driver at a second focus forming the detection zone where an external electric field is applied. This technique is known as Air-Biased Coherent Detection (ABCD). The detection setup exploits air [49] excited by an intense delayed probe pulse with intensity I_{ω_0} coupled with the transmitted THz field E_{THz} and an external electric field E_{bias} to generate a second laser harmonic component whose intensity obeys

$$I_{2\omega_0}(\tau) \propto \int \left[\chi^{(3)} I_{\omega_0}(t-\tau)\right]^2 E_{\mathrm{bias}} E_{\mathrm{THz}}(t)\,\mathrm{d}t. \quad (1)$$

Here, $\chi^{(3)}$ is the cubic nonlinear susceptibility component of air allowing frequency mixing (THz Field-Induced Second Harmonic (TFISH) generation [49,50]), while τ is the delay of the probe pulse. Alternating the amplitude of the bias electric field E_{bias} allows to measure the above second harmonic component and thus obtain the THz field in amplitude and phase [51]. Once the temporal shape of the THz pulse has been recorded, a Fourier transform yields its spectrum. Note that other plasma-based detection methods have been proposed for remote THz spectroscopy, such as the THz Radiation Enhanced Emission of Fluorescence (REEF) technique [52, 53]. Mainly exploiting variations in the UV plasma fluorescence by interaction with THz pulses, this method, although suitable to measure THz fields at $\sim$ 10-m standoff distances, has, however, so far provided limited exploitable bandwidths ($< 5-7$ THz) for efficient material characterization.

In this Letter, we provide a follow-up of the ALTESSE project [54] (Air Laser-based TErahertz SpectroScopy of Explosives), dedicated to acquiring spectral signatures of explosives or hazardous materials at large distances through plasma-based terahertz spectroscopy. The primary scientific goal of this project extension - named ALTESSE 2 - is to test the feasibility of THz spectroscopy of powders, mainly explosives, using *long* two-color ($800 + 400$ nm) plasma filaments as a THz source. The first part of this project [35] revealed the possibility of performing ABCD-based THz-TDS at distances from the laser source exceeding 10 m, but with the SH component and plasma produced just a few tens of cm before the sample. Here we demonstrate the possibility of measuring similar spectral signatures from up to 1 m long plasma filaments in air and performing reliable spectroscopy over meter-range distances ≥ 3 m. For experimental validation, the same samples have also been measured by a standard ABCD system, i.e., using much shorter plasmas created at 30 cm focusing distance from the laser exit under laboratory conditions. The measured transmission signals of

various samples reproduce the principal absorption peaks revealed in [35] in the 10-THz broad range. Furthermore, we investigate the impact of the thickness and concentration of the analyzed materials on the transmitted signal. Despite variations inherent to the sample preparation and fluctuations in the optical setups, we provide evidence that the main spectral fingerprints remain detectable from samples with increased thickness and concentration rates.

Experimental setup. – Our THz-ABCD spectroscopy setup – called 3-m THz-ABCD in the following – is schematically shown in fig. 1. A regeneratively amplified Ti:Sapphire laser system (Spitfire Pro, Spectra-Physics, 1 kHz repetition rate) with 800 nm central wavelength delivers FH pulses with 35 fs (FWHM) pulse duration, 1 cm diameter, and 4.4 mJ pulse energy - hence the peak power of the pulses (approximately 125 GW) is definitely above the critical power for self-focusing [37] in air or pure nitrogen. The laser beam, linearly polarized, is separated into pump and probe arms by a beam splitter (T:90, R:10). A focusing telescope, composed of two (concave and convex) lenses with focal lengths of -100 and 300 mm, respectively, is used to generate a plasma filament. Before the onset of plasma generation (nonlinear focus), about 3 m behind the second lens ($F = 300$ mm), the beam path passes through a system of flat mirrors. The plasma filament position can be controlled by varying the inter-mirror distance. After the telescope, the FH pump pulse (800 nm) is vertically polarized by a half-wave plate (HWP). It then passes through a 100 µm thick type-I barium borate (BBO) crystal to produce the SH pulse (400 nm) with $22-25\%$ conversion efficiency. A dual-wavelength half-wave plate (DHWP) ensures the SH polarization parallel to FH (800 nm). The two-color pulse is next focused into dry nitrogen, creating an approximately 150 mm long plasma filament. We note that up to 1 m long emissive plasmas can be produced using the alternative setup shown in fig. 5. The filamentary plasma generates luminescence in the blue region, between 300 and 450 nm (see bottom inset of fig. 1). The BBO crystal is placed 80 cm before the filament position to minimize the temporal walk-off between FH and SH [55] without inducing any damage in the BBO crystal. THz emission from the laser-induced plasma, optimized by adapting the position and angle of the BBO crystal [34, 56], is collimated and focused by a pair of parabolic mirrors P1 and P2 (4" and 2" focal length respectively). Mirror P1 is placed at 12 cm distance from the end of the filament, and the sample is located at the focal point of mirror P2. A high-resistivity silicon wafer is introduced between P1 and P2 to block the residual optical beam. The THz beam is collimated and refocused again by a pair of parabolic mirrors P3 and P4 (4" and 2" focal length, respectively). Mirrors P1 and P4 are drilled with a 3-mm diameter hole at their center.

To perform ABCD measurements, the FH probe pulse is guided through the hole of the parabolic mirror P4. The THz and probe pulses are focused between two electrodes of a high voltage (HV) module delivering a bias field with 6 kV/cm amplitude. The coupling between the optical probe beam, the THz beam, and the bias field creates a second harmonic component through the nonlinear Kerr response following eq. (1). Its intensity, proportional to the THz field, is finally selected by a bandpass filter and detected by an avalanche photodiode (APD). To avoid the absorption of THz waves by water in the surrounding air, a Plexiglas box is placed around the THz beam path and regularly purged with nitrogen. The standard ABCD system used as a reference to compare sample spectra acquired over short distances is detailed in [35, 57]. This classical ABCD setup – called 30-cm THz-ABCD – focuses two-color pulses at 30 cm from the laser exit, creating much shorter (~ 2.5 cm long) plasmas in the air.

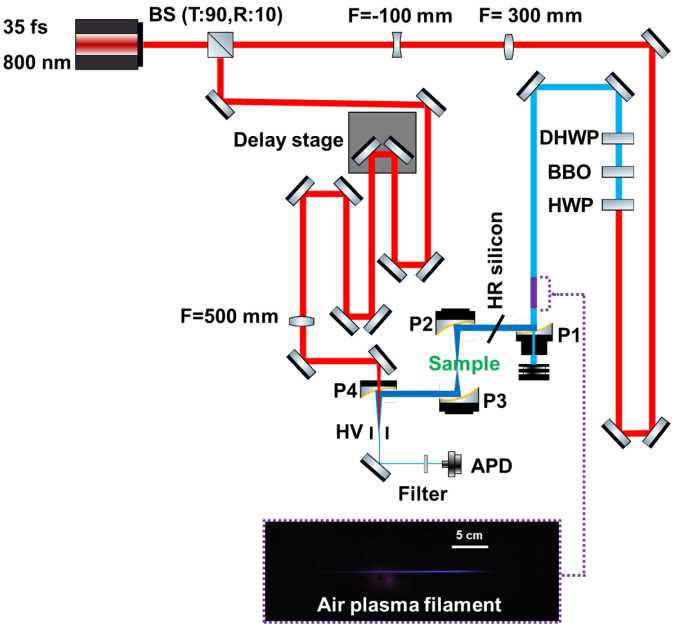

Fig. 1: Experimental setup of the ABCD detection system used in transmission. A two-color filament is generated 3 m behind the second lens ($F = 300$ mm), where the SH pulse is produced by a type-I BBO crystal. FH and SH trigger photocurrents (air plasma) responsible for THz emission in front of the parabolic mirror P1. The sample position is located at the focal point of parabolic mirror P2. The THz pulse is detected by the ABCD method that mixes the probe pulse, the transmitted THz pulse, and the bias electric field at the focus of P4.

The samples were prepared as powders mixed with polyethylene (PE) compressed into pellets with ~ 1 cm diameter and ~ 1 mm thickness, mounted on a sample holder. The recorded THz temporal signals obtained with and without the samples were Fourier transformed to get their characteristic spectra. Most samples were prepared within the baseline mass ratio $m_{\text{sample}}/m_{\text{PE}} = 1/9$. The analyzed compounds were the explosives TATB (2,4,6-triamino-1,3,5-trinitrobenzene), ANTA (3-Amino-5nitro-1,2,4-triazole), TNB (1,3,5-Trinitrobenzene), and the nucleobase thymine. We also performed spectroscopy of ni-

troguanidine [NGu - $(NH_2)_2CNNO_2$], a very insensitive but powerful explosive, for which we increased the mass ratios up to 1/2. Reversely, with the same material, we studied the influence of the sample thickness, which was increased up to 1.4 mm while keeping the concentration constant.

Results. – Figure 2 shows the THz waveforms (a) and their corresponding spectra (b) recorded by the 3-m THz-ABCD system as described above. Nitrogen 1 and 2 represent two consecutive reference measurements performed in a pure nitrogen atmosphere (without a sample) to quantify the stability and accuracy of our system. The spectra cover the frequency range up to ~ 35 THz, where the noise floor is reached, and exhibit a dominant contribution around 5 THz. The variation between the two consecutive measurements stays within 10%, suggesting reasonable stability of the 3-m THz-ABCD setup. However, we report reduced stability compared with standard ABCD systems based on two-color air plasmas of a few cm lengths as used, e.g., in [35]. Several factors can explain this reduced stability. Local instability of the plasma filament due to the competition between Kerr self-focusing and plasma defocusing and fluctuations caused by the nitrogen purge system may lead to variations in the generated THz signal along the ~ 15 cm plasma channel. Furthermore, it is difficult to collimate the entire THz beam. It is well known that the THz emission angle is usually confined below 10° [58,59], making the spatial separation between the optical and THz beams challenging. Particularly in filamentation geometry, nonlinear pulse propagation over an extended optical path fosters supercontinuum generation and broadening of the THz spectrum towards the pump spectrum at clamping intensity [39]. Therefore, we expect broader THz spectra, especially beyond 15 THz, with the 3-m THz-ABCD setup, as confirmed, e.g., by the reference spectra of Figs. 4(c,d). Although carrying lower energy, THz frequencies with small conical emission $< 1°$ [59,60] are more sensitive to the hole of the parabolic mirror P1 (see fig. 1), which may cause fluctuations in the output THz profile. In addition, the pump-probe experiments are less robust when the optical path is long. Likewise, the number of optical elements (mirrors) impacts the system stability because spatial and temporal synchronization becomes very sensitive to mechanical vibrations. Finally, the THz average power measured (at 25 Hz sampling frequency) after two silicon substrates – one located at the entrance of the powermeter (Gentec THZ-B-DZ detector) – is decreased to 15 μW, which is relatively low compared to the 100 μW of the standard system and may foster less stable THz spectra at high frequencies.

We evaluated the performance of our 3-m THz-ABCD setup in analyzing the different molecular crystals listed in the previous section. This evaluation is limited to spectral signatures in the frequency range from 0.2 to 10 THz to minimize the impact of the stability issues at frequencies > 10 THz mentioned above. Besides, scattering from sample powders renders absorption spectra noisy at high frequencies > 15 THz [35]. Figure 3(a) displays recorded THz waveforms obtained with and without an exemplary sample, ANTA. The reference signal is a single-cycle pulse having a duration of about 200 fs. The delay between both signals originates from the optical index of the sample material. In fig. 3(b), the transmitted THz spectrum with the ANTA sample shows strong absorption lines by phonon resonances.

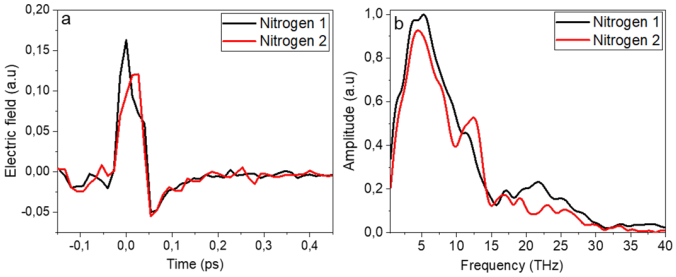

Fig. 2: (a) Measured THz waveforms in time domain obtained by ABCD spectroscopy from our 3-m THz-ABCD setup. (b) Amplitude spectra obtained by Fourier transform of (a). Nitrogen 1 and 2 correspond to two consecutive measurements performed in nitrogen with no sample.

Next, figs. 3(c)-(f) detail the absorption coefficients obtained for ANTA, TATB, thymine, and TNB for the baseline mass ratio $m_{\text{sample}}/m_{\text{PE}} = 1/9$. As in [35], we display the corresponding absorption coefficient

$$\alpha(\omega) = -\frac{2}{d} \ln \left[\frac{1}{T(n)} \left| \frac{E_{\text{sample}}(\omega)}{E_{\text{ref}}(\omega)} \right| \right] , \qquad (2)$$

where d denotes the sample thickness. The transmission factor $T(n) = 4n/(n+1)^2$ accounts for the Fresnel reflection loss at the pellet interfaces. We did not attempt an extraction of the refractive index $n(\omega)$ of the samples since the phase fluctuations of the detected signals were significant. Hence we assume a constant transmission factor across our spectral range. While it is well known that the refractive index n varies across the resonance bands observed here, the variation leads to only minor variations of $T(n)$. Red curves refer to data collected from the filament-based 3-m THz-ABCD setup. In contrast, the black curves show data measured from a two-color 2.5 cm long plasma formed with the 30-cm THz-ABCD system, similar to the laboratory setup used in [35]. We can observe in fig. 3(c) that the three main features at 1.94, 2.7, and 7 THz persist, despite the considerable differences in beam propagation (and plasma) geometry. These features correspond to the main absorption lines of ANTA reported in [35]. TATB [fig. 3(d)] shows a typical absorption spectrum with two main lines at 3.52 THz (intermolecular torsions) and 8.6 THz (intramolecular oscillations), always in agreement with the latter reference. TNB [fig. 3(f)] exhibits absorption lines at 3.86 and 4.74 THz, similar to those reported in [61]. Finally, Thymine [fig. 3(e)] reveals characteristic

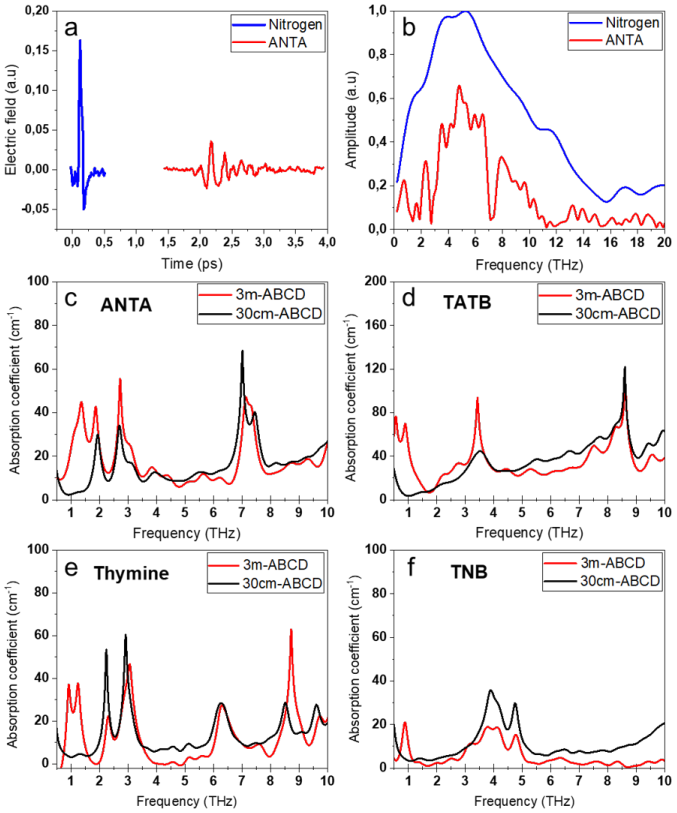

Fig. 3: (a) THz waveforms measured without (blue) or with sample (red curve) from the 3-m THz-ABCD system. (b) Amplitude spectra obtained by Fourier Transform. (c)-(f) Absorption coefficients obtained for samples of (c) ANTA, (d) TATB, (e) Thymine, and (f) TNB. Black curves show data acquired with the standard 30-cm THz-ABCD setup (see, e.g., [35]).

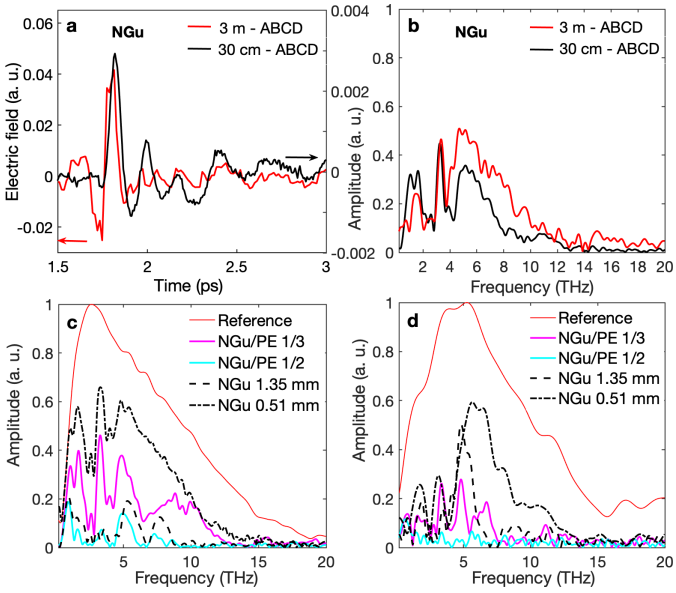

Fig. 4: Transmitted (a) THz fields and (b) spectra for the baseline configuration of Nitroguanidine (NGu) (80 mg mass) with 1 mm thickness and concentration of NGu/PE = 1/9. (c) Spectral amplitudes of four other NGu samples with either different concentrations [NGu/PE = 1/3, 1/2] or different thicknesses [0.51 mm and 1.35 mm] from the 30-cm THz-ABCD system. (d) Same information for the 3-m THz-ABCD setup. Red curves show the spectral amplitude of the reference THz pulse measured in pure nitrogen without a sample.

peaks at 2.23, 2.92, 6.27, and 8.51 THz, besides a smaller one at 9.62 THz. The same peaks were reported at 2.25, 2.95, 6.30, 8.50, and 9.60 THz in [62] and are also visible in [35]. The absorption coefficients are consistent with previous publications in the frequency range < 10 THz and prove that our 3-m THz-ABCD spectrometer can capture the major spectral signatures of each sample. These measurements confirm the reliability of THz-ABCD spectroscopy employing extended two-color filaments to detect and identify various materials, whether energetic or not.

Figure 4 details the transmitted electric fields [fig. 4(a)] and corresponding spectra [fig. 4(b)] of Nitroguanidine (NGu) in the baseline pellet preparation $m_{\mathrm{NGu}}/m_{\mathrm{PE}} = 1/9$ ($m_{\mathrm{NGu}} = 80$ mg) and 1 mm thickness, for the standard 30-cm ABCD-THz setup delivering a 2.5 cm short plasma and that employing a 15 cm long plasma formed at more than 3 m from the laser source. With the first setup we can identify the spectral absorption signatures at the transmission minima located at 1.34, 2.37, and 2.79 THz, which are very close to the absorption lines reported in [63]. With the second setup the latter two minima appear slightly shifted to 2.5 and 2.82 THz, respectively. We also studied the influence of the sample thickness between 0.51 and 1.35 mm for constant pellet diameter (1 cm) and concentration (NGu/PE = 1/9). Figure 4(c) shows that for the 30-cm setup, a decrease (increase) in the pellet thickness causes an increase (decrease) in the spectral amplitude of the main transmission peaks at 1.5 THz and 3.3 THz. Attenuation in the transmitted spectrum is accompanied by a reduction in the frequency bandwidth. A similar decrease is observed when increasing the concentration. Figure 4(d) presents similar data acquired with the 3-m setup. Here, we again observe a decrease in the transmitted spectral amplitude when the sample concentration is increased. The expected amplitude decrease for increasing sample thicknesses is, however, not always observed [compare, e.g., the NGu spectrum for the 1.35-mm thickness in fig. 4(d) with that of the 1-mm baseline sample in fig. 4(b)]. Moreover, none of the measurements presented in fig. 4 are compatible with the Beer-Lambert law. We attribute this finding to variability in the sample preparation, possibly inducing strong scattering effects, and to some instabilities in our 3-m ABCD setup. Nonetheless, the above data demonstrate that even though engaging only ~ 15 μW THz average power, the system remains sensitive enough to detect major spectral signatures and notable variations in the NGu concentration and sample thickness.

Finally, we mention that the above setup can easily be extended to form longer filament ranges through the more

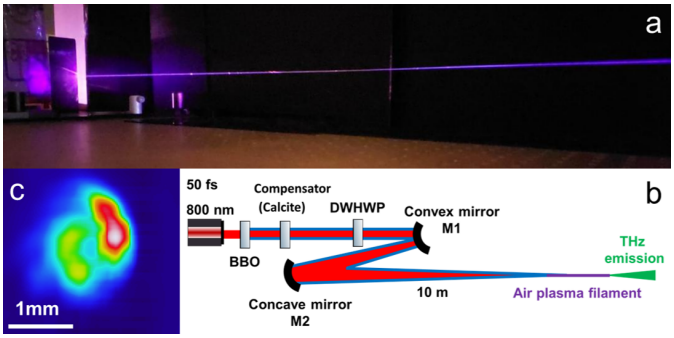

Fig. 5: (a) Photo of two-color filament created at 10 meters focusing distance. (b) Setup. (c) Measured THz beam profile.

straightforward setup sketched in fig. 5(b). This employs two parabolic mirrors providing a loosely focused propagation geometry for more energetic laser pulses. This setup successfully produced extended filamentation channels at the Institut de Recherche Franco-Allemand de Saint-Louis (ISL) with a more energetic laser source (12 mJ, 35 fs, 100 Hz repetition rate). The photo in fig. 5(a) shows a filament formed at 10 m of the optical table hosting the laser system. The 800 nm, 15-mm diameter, 10-12 mJ FH pulse passed through a 100-μm thick BBO crystal, creating the SH pulse with about 30% conversion efficiency. Both laser harmonics went through a calcite plate acting as time delay compensator (580-1000 fs). Careful delay adjustment guaranteed an overlap of FH and SH inside the plasma. The onset of the plasma channel occurred 10 m away from the laser exit, and the plasma fluorescence region covered 1 m along the optical path. Powermeter measurements (at 25 Hz sampling frequency) allowed us to measure up to $\sim 100\,\mu$W THz averaged power yields after two Si filters. An example of the THz beam profile measured with a THz camera and reflected by a parabolic mirror with 6-mm diameter hole filtering the optical pulse is displayed in fig. 5(c). This mirror was placed 20 cm from the plasma channel. No spectroscopy measurements were, however, performed during the ISL campaign.

Conclusion. – In summary, we have presented a proof of concept about the possibility of performing THz-ABCD spectroscopy with a THz beam emitted by extended (> 10 cm) plasma filaments generated by two-color laser pumps at more than 3 m from the laser source. A comparative study between this setup and a standard 30-cm THz-ABCD setup as used, e.g., in [35] demonstrates that extended filamentary plasmas can produce THz yields sufficient to capture the main characteristic absorption lines of different molecular materials. We also supplied variations in the THz spectral amplitude when the concentration or thickness of the sample varies. Although the stability of the present system from one measurement to another leaves room for improvement, our results remain very encouraging to perform THz-ABCD spectroscopy at remote distances.

* * *

Agence Innovation Défense (AID) and Agence Nationale de la Recherche (ANR-19-ASMA-0007); Grand Équipement National De Calcul Intensif (A0120507594); Qatar National Research Fund (NPRP 12S-0205-190047). The authors thank M. Allemand (Amplitude), Cl. Diboune (Imagine Optic), T. Goepfert (ISL) and L. Merlat (ISL) for technical assistance.

REFERENCES

[1] Tonouchi M., *Nat. Photon.*, **1** (2007) 97.
[2] Lewis R. A., *J. Phys. D: Appl. Phys.*, **47** (2014) 374001.
[3] Son J.-H., Oh S. J. and Cheon H., *J. Appl. Phys.*, **125** (2019) 190901.
[4] Wallace V., Fitzgerald A., Shankar S., Flanagan N., Pye R., Cluff J. and Arnone D., *British Journal of Dermatology*, **151** (2004) 424.
[5] Sim Y. C., Park J. Y., Ahn K.-M., Park C. and Son J.-H., *Biomed. Opt. Express*, **4** (2013) 1413.
[6] Cheon H., Paik J. H., Choi M., Yang H.-J. and Son J.-H., *Scientific Reports*, **9** (2019) 6413.
[7] Salén P., Basini M., Bonetti S., Hebling J., Krasilnikov M., Nikitin A. Y., Shamuilov G., Tibai Z., Zhaunerchyk V. and Goryashko V., *Physics Reports*, **836-837** (2019) 1.
[8] Novelli F., Guchhait B. and Havenith M., *Materials*, **13** (2020) 1311.
[9] Vella A., Houard J., Arnoldi L., Tang M., Boudant M., Ayoub A., Normand A., Da Costa G. and Hideur A., *Sci. Adv.*, **7** (2021) eabd7259.
[10] LaRue J. L., Katayama T., Lindenberg A., Fisher A. S., Öström H., Nilsson A. and Ogasawara H., *Phys. Rev. Lett.*, **115** (2015) 036103.
[11] Daranciang D., Goodfellow J., Fuchs M., Wen H., Ghimire S., Reis D. A., Loos H., Fisher A. S. and Lindenberg A. M., *Applied Physics Letters*, **99** (2011) 141117.
[12] Omidian M., Leitherer S., Néel N., Brandbyge M. and Kröger J., *Phys. Rev. Lett.*, **126** (2021) 216801.
[13] *Présentation de la ligne THz AILES du synchrotron SOLEIL (Saclay)* `https://www.synchrotron-soleil.fr/fr/lignes-de-lumiere/ailes`.
[14] Tammaro S., Pirali O., Roy P., Lampin J.-F., Ducournau G., Cuisset A., Hindle F. and Mouret G., *Nature Communications*, **6** (2015) 7733.
[15] Fisher A., Park Y., Lenz M., Ody A., Agustsson R., Hodgetts T., Murokh A. and Musumeci P., *Nature Photonics*, **16** (2022) 441.
[16] Burford N. M. and El-Shenawee M. O., *Optical Engineering*, **56** (2017) 1 .
[17] Richter P., Kartal E., Kohlhaas R. B., Semtsiv M. P., Schell M., Masselink W. T., Globisch B. and Koch M., *IEEE Transactions on Terahertz Science and Technology*, **10** (2020) 167.
[18] Faist J., Capasso F., Sivco D. L., Sirtori C., Hutchinson A. L. and Cho A. Y., *Science*, **264** (1994) 553.
[19] Gmachl C., Capasso F., Sivco D. L. and Cho A. Y., *Reports on Progress in Physics*, **64** (2001) 1533.

[20] Dean P., Valavanis A., Keeley J., Bertling K., Lim Y. L., Alhathlool R., Burnett A. D., Li L. H., Khanna S. P., Indjin D., Taimre T., Rakić A. D., Linfield E. H. and Davies A. G., *J. Phys. D: Appl. Phys.*, **47** (2014) 374008.

[21] Boyd R., *Nonlinear Optics* (Academic Press, San Diego) 2008.

[22] Hu B. B., Zhang X., Auston D. H. and Smith P. R., *Applied Physics Letters*, **56** (1990) 506.

[23] Rice A., Jin Y., Ma X. F., Zhang X., Bliss D., Larkin J. and Alexander M., *Applied Physics Letters*, **64** (1994) 1324.

[24] Blanchard F., Razzari L., Bandulet H. C., Sharma G., Morandotti R., Kieffer J. C., Ozaki T., Reid M., Tiedje H. F., Haugen H. K. and Hegmann F. A., *Optics Express*, **15** (2007) 13212.

[25] Zhang X., Ma X. F., Jin Y., Lu T., Boden E. P., Phelps P. D., Stewart K. R. and Yakymyshyn C. P., *Applied Physics Letters*, **61** (1992) 3080.

[26] Hauri C. P., Ruchert C., Vicario C. and Ardana F., *Applied Physics Letters*, **99** (2011) 161116.

[27] Vicario C., Monoszlai B. and Hauri C., *Phys. Rev. Lett.*, **112** (2014) 213901.

[28] Shalaby M., Vicario C., Thirupugalmani K., Brahadeeswaran S. and Hauri C., *Opt. Lett.*, **41** (2016) 1777.

[29] Nahata A., Weling A. S. and Heinz T. F., *Applied Physics Letters*, **69** (1996) 2321.

[30] Hebling J., *Optical and Quantum Electronics*, **28** (1996) 1759.

[31] Hebling J., Almási G., Kozma I. Z. and Kuhl J., *Opt. Express*, **10** (2002) 1161.

[32] Yeh K. L., Hoffmann M. C., Hebling J. and Nelson K. A., *Applied Physics Letters*, **90** (2007) 171121 yeh, K.-L. Hoffmann, M. C. Hebling, J. Nelson, Keith A.

[33] Fülöp J. A., Ollmann Z., Lombosi C., Skrobol C., Klingebiel S., Pálfalvi L., Krausz F., Karsch S. and Hebling J., *Opt. Express*, **22** (2014) 20155.

[34] Kim K. Y., Taylor A. J., Glownia J. H. and Rodriguez G., *Nat. Photon.*, **2** (2008) 605.

[35] Bergé L., Kaltenecker K., Engelbrecht S., Nguyen A., Skupin S., Merlat L., Fischer B., Zhou B., Thiele I. and Jepsen P. U., *Eur. Phys. Lett.*, **126** (2019) 24001.

[36] Matsubara E., Nagai M. and Ashida M., *Applied Physics Letters*, **101** (2012) 11105.

[37] Bergé L., Skupin S., Nuter R., Kasparian J. and Wolf J.-P., *Reports on Progress in Physics*, **70** (2007) 1633.

[38] Braun A., Korn G., Liu X., Du D., Squier J. and Mourou G., *Opt. Lett.*, **20** (1995) 73.

[39] Bergé L., Skupin S., Köhler C., Babushkin I. and Herrmann J., *Phys. Rev. Lett.*, **110** (2013) 073901.

[40] D'Amico, C. and Houard, A. and Franco, M. and Prade, B. and Mysyrowicz, A. and Couairon, A. and Tikhonchuk, V. T., *Phys. Rev. Lett.*, **98** (2007) 235002.

[41] Daigle J.-F., Théberge F., Henriksson M., Wang T.-J., Yuan S., Châteauneuf M., Dubois J., Piché M. and Chin S. L., *Optics Express*, **20** (2012) 6825.

[42] Clerici M., Peccianti M., Schmidt B. E., Caspani L., Shalaby M., Giguère M., Lotti A., Couairon A., Légaré F., Ozaki T., Faccio D. and Morandotti R., *Phys. Rev. Lett.*, **110** (2013) 253901.

[43] Wang T.-J., Yuan S., Chen Y., Daigle J.-F., Marceau C., Théberge F., Châteauneuf M., Dubois J. and Chin S. L., *Applied Physics Letters*, **97** (2010) 111108.

[44] González de Alaiza Martínez P., Babushkin I., Bergé L., Skupin S., Cabrera-Granado E., Köhler C., Morgner U., Husakou A. and Herrmann J., *Phys. Rev. Lett.*, **114** (2015) 183901.

[45] Han P. Y. and Zhang X.-C., *Meas. Sci. Technol.*, **12** (2001) 1747.

[46] Fattinger C. and Grischkowsky D., *Applied Physics Letters*, **53** (1988) 1480.

[47] Wu Q. and Zhang X. C., *Applied Physics Letters*, **67** (1995) 3523.

[48] Leitenstorfer A., Hunsche S., Shah J., Nuss M. C. and Knox W. H., *Appl. Phys. Lett.*, **74** (1999) 1516.

[49] Dai J., Xie X. and Zhang X.-C., *Phys. Rev. Lett.*, **97** (2006) 103903.

[50] Cook D. J., Chen J. X., Morlino E. A. and Hochstrasser R. M., *Chemical Physics Letters*, **309** (1999) 221.

[51] Karpowicz N., Dai J., Lu X., Chen Y., Yamaguchi M., Zhao H., Zhang X.-C., Zhang L., Zhang C., Price-Gallagher M., Fletcher C., Mamer O., Lesimple A. and Johnson K., *Applied Physics Letters*, **92** (2008) 011131.

[52] Liu J., J. D., S. L. C. and Zhang X.-C., *Nat. Photonics*, **4** (2010) 627.

[53] Clough B. and Zhang X.-C., *Frontiers of Optoelectronics*, **7** (2014) 199.

[54] *ANR MATURATION ALTESSE 2* `https://anr.fr/Projet-ANR-19-ASMA-0007`.

[55] Nguyen A., de Alaiza Martínez P. G., Déchard J., Thiele I., Babushkin I., Skupin S. and Bergé L., *Opt. Express*, **25** (2017) 4720.

[56] Kim K.-Y., Glownia J. H., Taylor A. J. and Rodriguez G., *Opt. Express*, **15** (2007) 4577.

[57] Tarekegne A. T., Zhou B., Kaltenecker K., Iwaszczuk K., Clark S. and Jepsen P. U., *Optics Express*, **27** (2019) 3618.

[58] You Y. S., Oh T. I. and Kim K. Y., *Phys. Rev. Lett.*, **109** (2012) 183902.

[59] Andreeva V. A., Kosareva O. G., Panov N. A., Shipilo D. E., Solyankin P. M., Esaulkov M. N., González de Alaiza Martínez P., Shkurinov A. P., Makarov V. A., Bergé L. and Chin S. L., *Phys. Rev. Lett.*, **116** (2016) 063902.

[60] Rasmussen M., Nagy O., Skupin S., Stathopulos A., Bergé L., Jepsen P. U. and Zhou B., *Optics Express*, **31** (2023) 9287.

[61] Engelbrecht S., Bergé L., Skupin S., Wang T., Jepsen P. U. and Fischer B. M., *40th International Conference on Infrared, Millimeter, and Terahertz waves (IRMMW-THz), Hong Kong, China*, (2015) 1.

[62] Yu M., Yan S., Sun Y.-Q., Sheng W., Tang F., Peng X.-Y. and Hu Y., *Sensors*, **19** (2019) 1148.

[63] Chen J., Chen Y., Zhao H., Bastiaans G. J. and Zhang X.-C., *Optics Express*, **15** (2007) 506.